Solar Coronal Holes and Open Magnetic Flux

A Tale of 248 Carrington Rotations

Lowder, C.[1], Qiu, J.[1], Leamon, R.[1], Longcope, D.[1]
1:Department of Physics, Montana State University

MONTANA STATE UNIVERSITY
SOLAR PHYSICS

Abstract

Using SDO/AIA and STEREO/EUVI EUV data in conjunction with an instrument-specific adaptive intensity thresholding algorithm, we are able to track coronal hole boundaries across the entire solar surface at a cadence of 12 hours. SOHO/EIT provides earlier era data, allowing the building of EUV coronal hole maps over the course of a solar rotation. We find that for solar cycle 23 the unsigned magnetic flux enclosed by coronal hole boundaries ranges from $(2-5)x10^{22}Mx$, covering 5%-17% of the solar surface. For solar cycle 24 this flux ranges from $(2-4)x10^{22}Mx$, covering 5%-10% of the solar surface. Using a surface flux transport model, we compare observational coronal hole boundaries and computed potential open field for solar cycles 23 and 24. From both our observed coronal holes and modeled open magnetic field, we find that low-latitude regions contribute significantly to the total open magnetic flux, and should be considered in more significant detail.

STEREO, where are you?

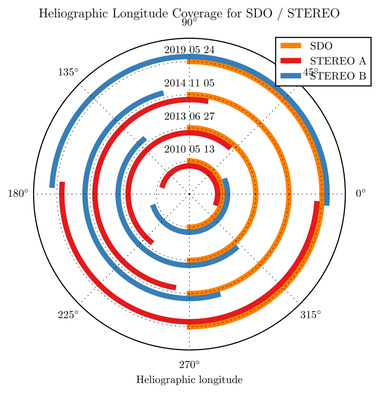

Figure 1: *Heliographic longitudinal location of SDO (yellow), STEREO A (red), and STEREO B (blue) at the time of SDO launch, 26 June 2013, 5 November 2014, and 24 May 2019.*

The two STEREO spacecraft, separated in their orbits, drift slowly ahead and behind our relative view of the sun from Earth. By taking advantage of the unique positioning of these spacecraft, and the EUV imagers on-board, we can construct nearly full surface maps of coronal hole boundaries.

These maps are not limited in cadence by rotation, and can be observed at cadences up to a few minutes for more detailed studies. For our long-term observations, we use a cadence of 12-hours.

- Note a lack of complete far-side coverage near SDO launch
- 24 May 2019 marks the ending of complete far-side coverage... which will continue for quite some time.

Mapping coronal hole boundaries

To map coronal hole boundaries, we employ the following intensity thresholding routine:

- For each instrument and time-step:
  - Partition image into subframes
  - Calculate local minimum values
  - Discard error values and pick median
  - Apply threshold to entire FOV
- Stitch together potential CH boundaries
- Overlay mask on MDI/HMI B_r
- Calculate magnetic flux pixel skew for each distinct potential CH region
- Discard unskewed regions as filament channels

With this method we are able to calculate a coronal hole map either built up over one full rotation for SoHO:EIT data. For the combination of STEREO:EUVI and SDO:AIA data, a nearly full-surface coverage map of coronal holes is calculated every 12 hours.

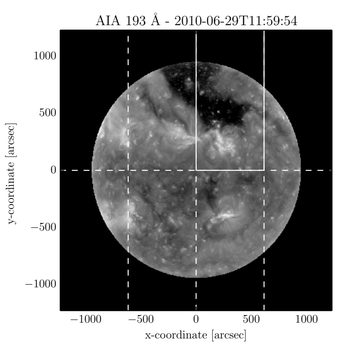

Figure 2: *Full-disk EUV data taken at 193Å by the AIA instrument aboard SDO. Boxes illustrate individual partitions for intensity thresholding. Solid box indicates the partial FOV in Figure 3.*

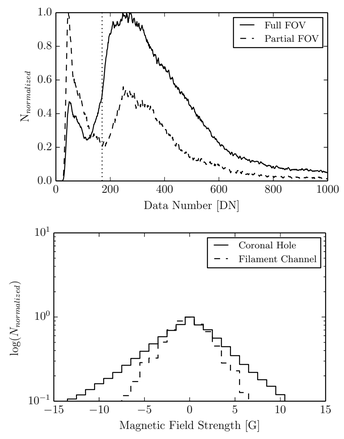

Figure 3: *EUV intensity histograms for the full and partial FOV displayed in Figure 2.*

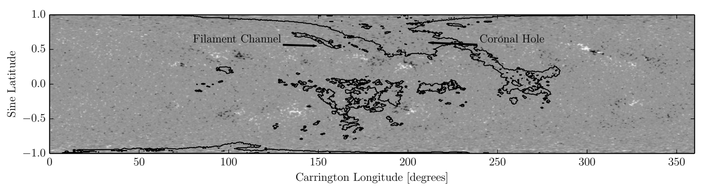

Figure 4: *Thresholded regions overlaid with a radial map of magnetic flux density from HMI for CR2098. A filament channel and coronal hole are identified for comparison. Filament channel regions are removed from the final coronal hole map.*

Time and relative dimension

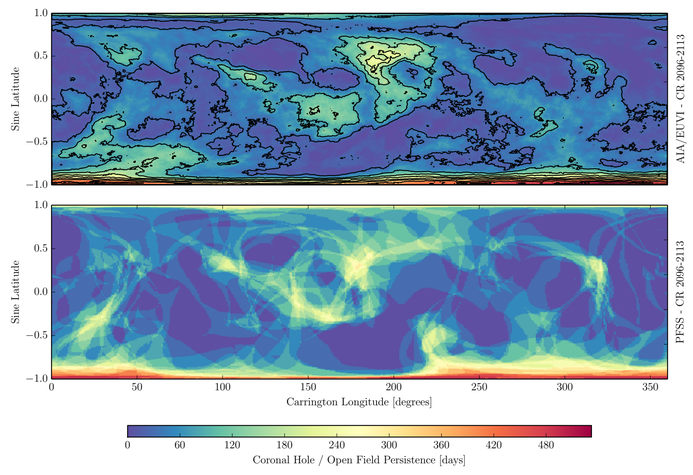

Figure 5: *Coronal hole persistence map for a combination of AIA 193Å and EUVI 195Å datasets, along with a corresponding map generated using spherical harmonic coefficients obtained from the Wilcox Solar Observatory and a PFSS open field reconstruction. Persistence is scaled in days of non-consecutive persistence of coronal hole / open field for each pixel. Contours are marked at equivalent WSO PFSS cadence.*

To compare our coronal hole and open magnetic field boundaries, we can consider the spatial distribution as well as the temporal. By combining AIA/EUVI data, we are able to generate a nearly full-surface map of coronal hole boundaries. To compare our observed boundaries to calculated open field boundaries, we can stack each surface boundary map in time.

$$\Psi(\theta_i, \phi_j) = \sum_k \psi(\theta_i, \phi_j, t_k) \tag{1}$$

The result is a latitude-longitude map, displaying the non-consecutive coronal hole 'persistence' at that location. These are useful as a comparative tool of boundary distribution over a small time period. Note the similar features between our CH map and WSO potential open field, especially the polar distribution of open field.

Surface open magnetic flux

To compare the magnetic flux between open field regions and coronal holes, we can construct a mask of each set of boundaries. These masks can then be overlaid on corresponding magnetic field data to compute the enclosed open magnetic field.

$$\Phi_{open}(t_k) = R_\odot^2 \sum_{i,j} \psi(\theta_i, \phi_j, t_k) \cos(\theta_i) B_r(\theta_i, \phi_j, t_k) \tag{2}$$

The upper panel of Figure 6 displays the northern and southern sunspot number in red and blue. Below is the total unsigned open photospheric magnetic flux, for a variety of observations. Coronal hole enclosed flux is calculated and displayed in solid curves for EIT and AIA/EUVI data in red and blue, respectively. Open photospheric magnetic flux is displayed for the non-potential model and our WSO potential field extrapolation in green and black, respectively. A yearly equivalent IMF field is displayed in orange, with the shaded region displaying the range of IMF values over that year.

The bottom three panels display similar data, broken into latitudinal zones. The second, third, and fourth panel indicate the northern polar, low-latitudinal, and southern polar flux and area data. Here we have defined $\pm$ 65 degrees as the polar cutoff angle.

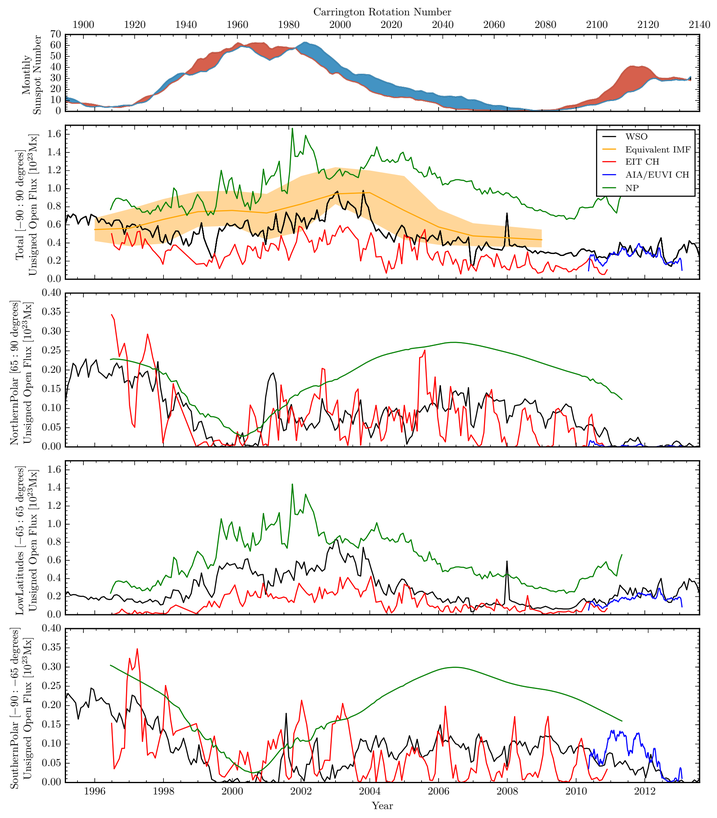

Figure 6: *Coronal hole and open magnetic field unsigned flux displayed for a variety of datasets.*

We can note a few aspects of this:

- Our EIT dataset underestimates the low-latitude flux and area. This is to be expected from our study of the dataset which yielded less contrast in distinguishing coronal hole boundaries.
- AIA-EUVI data matches the calculated magnetic fluxes from our WSO potential field extrapolation.
- The non-potential model overestimates the low-latitude open flux, but has slightly better agreement in the poles.

Flux transport model

We have developed a simple flux transport model, evolving an initial field from WSO data using Equation 3 to evolve the field. The source term is computed from MDI observations of dipole centroids.

$$\frac{\partial B_r}{\partial t} = D\nabla^2 B_r - \nabla \cdot (\mathbf{u} B_r) + S(t), \tag{3}$$

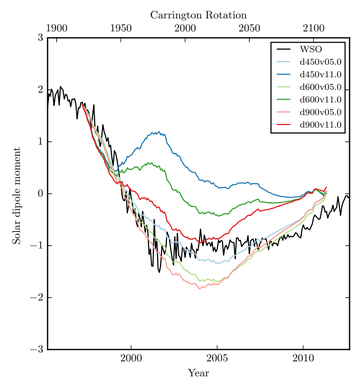

Figure 7: *Solar dipole moment for FTM parameters compared with a reference WSO potential field.*

- Parameter values to match dipole moment are in line with expected values.
- Higher meridional flow stunts the evolution of the dipole moment, resulting in higher low-latitude open field.

Surface magnetic flux

The total surface unsigned magnetic flux is defined as,

$$\Phi(R_\odot, t_k) = R_\odot^2 \sum_{i,j} \cos(\theta_i) B_r(\theta_i, \phi_j, t_k). \tag{4}$$

From this for each rotation the model surface flux can be compared with corresponding WSO observations reconstructed from harmonic coefficients. Here we have weighted the lower order harmonics to remove ringing and banding effects in the reconstructed field.

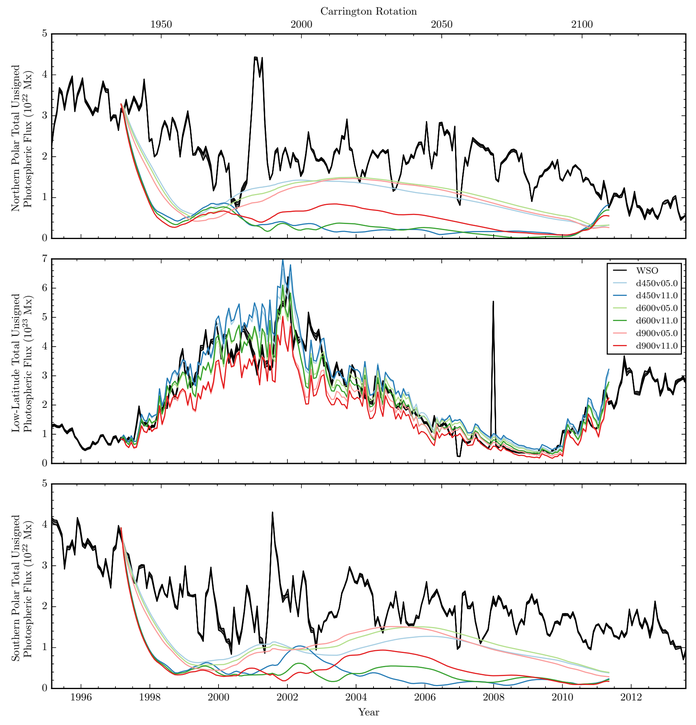

Figure 8: *Unsigned photospheric flux values from our flux transport model, compared with a band of values for reconstructed field from WSO. Photospheric flux is subdivided into latitude bands of [-90:-55], [-55:55], and [55:90] degrees.*

- Low latitude photospheric fluxes are in good agreement with WSO observations.
- Higher meridional flow profiles result in the polar field dropping off quickly, never to fully recover.

Bringing everything together

- The combination of AIA and EUVI datasets allows for nearly full-surface observations of coronal hole boundaries. The study of far-side coronal hole boundary evolution is possible with this methodology.
- These observations of CH boundaries guide the development of our flux transport model, especially with regard to low-latitude open magnetic flux and CH boundary evolution.
- Further study with a non-potential model is in progress, though with higher computational constraints.

References

- Krista, L. D. & Gallagher, P. T. 2009, SoPh, 256, 87-100
- Lowder, C., Qiu, J., Leamon, R. & Liu, Y. 2014, ApJ, 783, 142
- Wang, Y.-M. 2009, Space Science Reviews, 144, 383-399
- Yeates, A. R., Mackay, D. H., van Ballegooijen, A. A. & Constable, J. A. 2010, JGR, 115, 9112

Acknowledgments

Dick Canfield and Duncan Mackay have provided a great deal of discussion and valuable insight on this project.

This work is supported by NASA grant NNX13AG09G and NSF grant ATM-0748428.